J. Fluid Mech. (2017), *vol.* 818, R4, doi:10.1017/jfm.2017.168

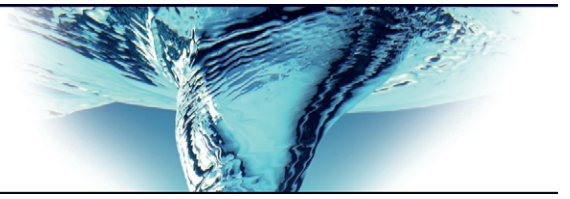

JFM RAPIDS
journals.cambridge.org/rapids

Mixing in continuous gravity currents

Diana Sher[1] **and Andrew W. Woods**[1,†]

[1]BP Institute, University of Cambridge, Madingley Road, Cambridge CB3 0EZ, UK

(Received 11 November 2016; revised 2 March 2017; accepted 3 March 2017;
first published online 6 April 2017)

We present measurements of the entrainment of ambient fluid into high-Reynolds-number gravity currents produced by a steady flux of buoyancy. The currents propagate along a horizontal channel and the mixing is measured using a light attenuation technique to obtain the cross-channel average of the density throughout the current. The total volume of the current increases linearly with time, at a rate in the range $(1.8–2.1)Q_o$ for source Froude numbers, Fr_o, in the range 0.1–3.7, where Q_o is the source volume flux per unit width. Most mixing occurs either immediately downstream of the inflow or near the head of the flow, with an increasing proportion of the entrainment occurring in a mixing zone near the inflow as Fr_o increases. A vertical gradient in the density and horizontal velocity develops in this mixing zone. This enables relatively dense fluid at the base of the current to catch up with the head, where it rises and mixes with the ambient fluid which is displaced over the head. The mixed fluid continues forward more slowly than the head, forming the relatively dilute fluid in the upper part of the current. Our data show that the depth and the depth-averaged buoyancy are primarily dependent on the position relative to the front, with the speed of the front being $\lambda(Fr_o)B_o^{1/3}$, where B_o is the source buoyancy flux per unit width. Here, $\lambda(Fr_o)$ increases from 0.9 to 1.1 as Fr_o increases from 0.1 to 3.7, while the Froude number at the head of the flow has a value of 1.1 ± 0.05.

Key words: gravity currents, mixing

1. Introduction

Gravity currents form when dense fluid, released from a localised source, spreads over a horizontal boundary, displacing a less dense fluid (Chen 1980; Simpson 1997; Huppert 2006). Experimental and theoretical research has explored the dynamics of gravity currents produced following the release of a finite mass (Huppert & Simpson 1980; Rottman & Simpson 1983; Bonnecaze, Huppert & Lister 1993; Sher & Woods 2015) and a continuous flux (Maxworthy 1983; Grundy & Rottman 1986; Bonnecaze *et al.* 1993; Gratton & Vigo 1994; Johnson & Hogg 2013) of dense fluid. There

†Email address for correspondence: andy@bpi.cam.ac.uk

is a good understanding of the scaling laws for the speed of the front of such currents (Britter 1979; Britter & Linden 1980; Huppert & Simpson 1980). Moreover, in finite-release currents, it is known that a considerable mass of ambient fluid is mixed into the flow (Hallworth *et al.* 1993, 1996; Hacker, Linden & Dalziel 1996; Marino, Thomas & Linden 2005; Ottolenghi *et al.* 2016), primarily through the head of the current (Samasiri & Woods 2015; Sher & Woods 2015). The mixing leads to the formation of a stratified flow which becomes progressively more dilute and is approximately self-similar, until bottom friction begins to dominate. For gravity currents produced by a constant flux of buoyancy, less is known about the role of the head on the mixing with ambient fluid and the associated dilution of the flow. Most theoretical models neglect mixing and assume that the motion is controlled by the shallow water equations, in which, as a further implicit simplification, the velocity and density are assumed to be uniform with depth (Grundy & Rottman 1986, Bonnecaze *et al.* 1993, Gratton & Vigo 1994, Slim & Huppert 2008, Hogg, Nasr-Azadani, Ungarish & Meiburg 2016). Recently, these models have been extended to include some mixing through the upper surface of the flow (Johnson & Hogg 2013), using the classical entrainment models of Ellison & Turner (1959) for the local entrainment across a horizontal density interface, assuming that the speed of the flow at the nose equals the speed of the nose, so that there is no mixing in the head. There are also some experimental observations of the mixing and deepening of the flow in an adjustment region near the inflow (Nourmohammadi, Afshin & Firoozabadi 2011, Chowdhury & Testik 2014, Najafpour *et al.* 2014), and measurements reported by Varjavand *et al.* (2015) have shown that there is a significant vertical gradient in density and velocity in such currents. However, little is known about the relative rates of mixing (1) in the inflow region, (2) in the head of the current and (3) along the upper surface of the flow, or how these evolve in time. The purpose of the present paper is to report new experiments in which we measure the mixing and the associated flow structure in a continuous gravity current. We use a combination of dye studies and light attenuation measurements to quantify how the relative amounts of mixing near the inflow and the head change as a function of the source Froude number. We also show that at long times, the distribution of fluid and buoyancy throughout the current is approximately self-similar.

2. Experiments

We carried out a series of experiments to study the motion of two-dimensional gravity currents produced by a constant source of buoyancy supplied to a tank of dimensions 500 cm × 10 cm × 50 cm (figure 1). The tank was filled with a layer of fresh water of depth 40 cm. Using a Nocchi pump, the current fluid was supplied from a source tank, filled with aqueous salt solution of buoyancy g'_o, with a volume flow rate of $Q_o w_o$, where the width of the tank was $w_o = 10$ cm. Before entering the main experimental tank, the flow passed through a series of flow straighteners, consisting of a 15 cm long series of parallel channels, each of square cross-section 1 cm × 1 cm, divided by spacers of thickness less than 1 mm, and of total cross-section 4 cm × 10 cm (figure 1). From here, the flow issued directly into the base of the experimental tank. This led to a repeatable and well-defined source for the gravity current, characterised in terms of the source buoyancy flux, $B_o = g'_o Q_o$, per unit width, and source Froude number,

$$Fr_o = \frac{u_o}{(g'_0 h_0)^{1/2}}, \tag{2.1}$$

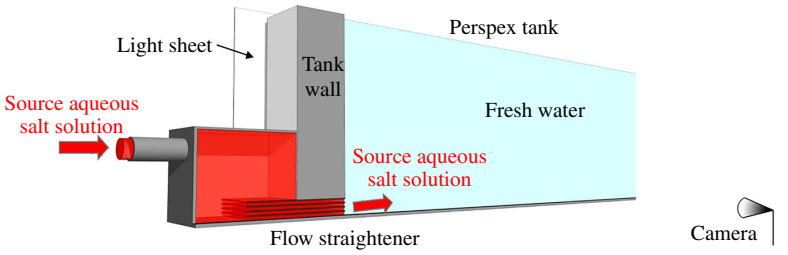

FIGURE 1. Schematic of the experimental set-up.

Exp.	$Q_o w_o$ (cm^3 s^{-1})	g'_o (cm s^{-2})	Re	Fr_o	Exp.	$Q_o w_o$ (cm^3 s^{-1})	g'_o (cm s^{-2})	Fr_o
A	343.3	118.9	6 400	0.1	B1	275.0	63.0	0.4
B	270.0	63.0	5 900	0.4	J1	600.0	5.2	2.7
C	145.0	15.3	2 700	0.5	B2	271.7	63.0	0.4
D	500.0	63.0	11 200	0.7	J2	491.7	5.2	2.7
E	680.0	63.0	14 000	1.0	B3	221.7	63.0	0.4
F	483.3	31.6	10 300	1.1	D3	491.7	63.0	0.7
G	680.0	31.6	11 600	1.5	E3	573.3	63.0	1.0
H	338.3	5.2	7 200	1.8	G3	638.3	31.6	1.5
I	660.0	12.0	15 100	2.3	H3	350.0	5.2	1.8
J	508.3	5.2	11 500	2.7	I3	653.3	12.0	2.3
K	678.3	5.2	14 600	3.7	J3	500.0	5.2	2.7

TABLE 1. Range of experimental conditions.

where $h_0 = 4$ cm is the depth of the inflow opening and $u_o = Q_o/h_o$ is the inflow speed, averaged over the cross-sectional area of the flow straighteners. A systematic series of experiments was carried out in which B_o and Fr_o were varied by using different values of Q_o and g'_o, and these are listed in table 1. In the experiments, the source volume flux was chosen so that the currents were of high Reynolds number, >3000, as defined by $Re = Q_o/\nu$, where ν is the kinematic viscosity of water, of magnitude 10^{-6} m^2 s^{-1}.

The tank was backlit using a Matrix LED light panel (W&Co. Displays and Signs) to provide a near uniform light source for the dye attenuation experiments used to measure the mixing, following the original approach of Cenedese & Dalziel (1998). In order to measure the mixing, a known mass of red TRS food dye was added to each unit volume of source water. As the gravity current mixed with the fluid in the tank, the concentration of dye decreased, leading to a reduction in the light attenuation across the width of the tank. The light intensity was converted to salt concentration using a calibration curve obtained by measuring the light attenuation of 15 known diluted mixtures of source fluid (Cenedese & Dalziel 1998, Sher & Woods 2015). The digital images were obtained using a Nikon D90 camera located on the opposite side of the tank to the light sheet. During the experiments, photographs were taken at regular time intervals in the range 0.25–1 s. The measurements of the total salinity at each time during the experiment were within 6 wt% of the actual mass of salt supplied to the tank at that time. In some additional experiments, dye was added to the current or the ambient fluid to visualise the flow pattern and process of mixing, and in further

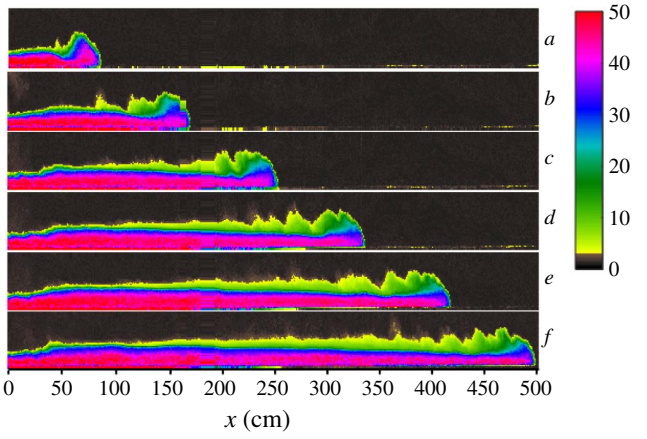

FIGURE 2. Series of images illustrating the evolution of the concentration field in the current as it advances along the flume (experiment G). The images are shown in false colour to illustrate the dilution of the flow relative to the original source fluid. The scale bar indicates the mass of salt per unit mass of the current (g kg^{-1}).

experiments, vertical lines of dye were injected into the flow. By following the motion of each of these lines of dye, we could estimate the vertical profile of the horizontal velocity (cf. Cafiero & Woods 2016). This enabled us to estimate the volume flux entrained into the flow in the near-source mixing zone.

3. Experimental results

A typical example of an advancing gravity current supplied by a constant source of buoyancy, experiment G, with $Fr_o = 1.5$, is shown in figure 2. The series of false-colour images represent the evolution of the density in the flow, with the colour scale representing the mass of salt in the fluid per unit mass of fluid, measured in g kg^{-1}. Just downstream of the source, in the first 40–50 cm of the flow, the current deepens and the upper part of the current becomes diluted by mixing with ambient fluid. Further downstream, the current has a relatively dense lower region which appears to reach the head of the flow, where a second region of mixing can be seen in the upper part of the head of the flow. This also appears to contribute to a region of relatively dilute fluid which forms on the upper surface of the flow.

In order to explore the mixing processes in more detail, in figure 3 we present four panels of images (*a–d*) for currents with $Fr_o = 2.7$ (*a*,*b*) and 0.4 (*c*,*d*), in which (*a*,*c*) the source fluid was initially dyed yellow, and then green, and (*b*,*d*) the ambient fluid initially ahead of the current included parcels of fluid dyed red, green and yellow. In figure 3(*a*), the time series of images illustrates that once the source fluid is dyed green, the green fluid advances through the lower part of the current to the front of the flow, and there appears to be little mixing between the green and yellow fluid as the flow advances. On reaching the head of the flow, the dense (green) fluid circulates upwards (cf. figures 2, 3*e*). In figure 3(*b*), it is seen that this fluid mixes with the ambient fluid originally ahead of the flow, to form an upper mixed layer which gradually lags behind the head of the flow since it travels forward more slowly than the continuing head (figures 2, 3*a*,*b*). The strong vertical stratification in the flow is produced by a combination of mixing near the inflow, which has some similarities

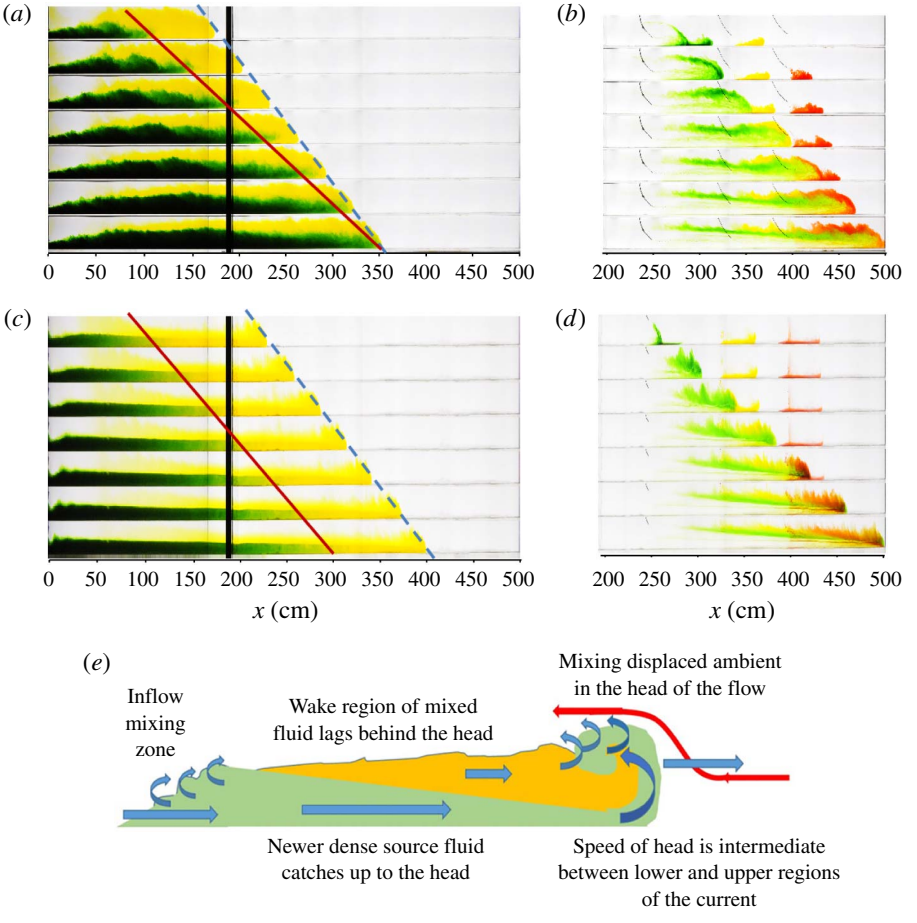

FIGURE 3. (*a*) Series of images illustrating the path followed by the source fluid as a function of time, visualised by changing the colour of the source fluid from yellow to green 5 s after the start of the experiment (experiment J1). The time series illustrates the strong vertical shear in the flow, as the green fluid runs below the yellow fluid towards the nose of the flow. The sloping red line illustrates the advance of the green dye front with time while the sloping dotted blue line indicates the advance of the head. The dense green fluid circulates upwards on reaching the head of the flow. (*b*) Series of images illustrating the evolution of regions of green, yellow and red dye originally located in the ambient fluid downstream of the current, in the case with $Fr_o = 2.7$ (experiment J2). As the head of the current passes by, the dyed ambient fluid is displaced upwards, and a fraction of the fluid is mixed into the recirculating current fluid. The successive regions of dye become vertically layered and strongly sheared out, as the dye that mixes into the upper part of the head is carried downstream in the wake of the current. (*c*) Series of images as in panel (*a*) but now with $Fr_o = 0.4$ (experiment B1). Here, the green source fluid advances more slowly towards the head of the current than in the case with higher source Froude number (panel *a*). (*d*) Series of images illustrating the evolution of regions of green, yellow and red dye originally located in the ambient fluid downstream of the current, with $Fr_o = 0.4$ (experiment B2). (*e*) Schematic of the flow processes in a steady gravity current.

to an internal hydraulic jump, and the head of the flow, where there appears to be a second phase of mixing. As a result, the fluid in the current undergoes a net circulation relative to the head as the current advances along the flume (figure 3*b*,*e*).

With a smaller source Froude number, the process is similar but the quantitative details are different. Indeed, figure 3(*c*,*d*) corresponds to a similar set of dye experiments to figure 3(*a*,*b*), but with $Fr_o = 0.4$. Figure 3(*c*), in which the colour of the source fluid was again changed from yellow to green, illustrates that the rate at which the fluid in the lower part of the current advances towards the head of the flow is more gradual than in figure 3(*a*). Indeed, the relative gradients of the sloping red line and the sloping blue line indicate the speed of advance of the green dye front relative to that of the head of the current. In figure 3(*d*), it is seen that the mixture of displaced ambient fluid, dyed green, yellow and red, with the fluid in the head of the flow penetrates much of the head.

3.1. *Speed of the head*

One of the key properties of a gravity current is the speed of the head of the current, $\mathrm{d}x_n/\mathrm{d}t$. From dimensional analysis, we expect this to scale with $B_o^{1/3}$, although, as seen in figure 4(*a*), there is also a weak dependence on Fr_o,

$$\frac{\mathrm{d}x_n}{\mathrm{d}t} = \lambda(Fr_o)B_0^{1/3}, \tag{3.1}$$

where λ may be approximated by the relation (figure 4*b*)

$$\lambda = 0.85 + 0.17Fr_o \quad \text{for } Fr_0 < 1 \quad \text{and} \quad \lambda = 1.1 \pm 0.1 \quad \text{for } Fr_0 > 1.0. \tag{3.2a,b}$$

We also measured the vertical integral of the buoyancy, $\overline{g'h}_n$, just behind the head of the flow, at the point where h has its maximum, h_n. The ratio of the speed of the nose, $\mathrm{d}x_n/\mathrm{d}t$, and $(\overline{g'h}_n)^{1/2}$ yields an estimate for the Froude number of the front of the current, Fr_n. Figure 4(*c*) shows that $Fr_n \approx 1.1 \pm 0.05$ for $0.1 < Fr_o < 3.7$.

3.2. *Mixing near the inflow*

Once the incoming jet of saline water entered the base of the tank, a local zone of flow adjustment and mixing developed. This region extended a distance of order 30–70 cm into the tank, increasing with the source Froude number. Beyond this zone, the current depth evolved much more slowly with distance down the tank. Examples of the inflow adjustment are shown in figure 5 for the cases (*a*) $Fr_o = 2.7$ and (*b*) $Fr_o = 0.4$. In the case $Fr_o = 2.7$, the current deepens over a distance of approximately 70 cm, with a significant amount of turbulent mixing apparent on the upper surface of the flow. Further downstream, the depth then evolves more gradually. In the case $Fr_o = 0.4$, the current initially accelerates and thins out, but then it appears to deepen and mix across its upper surface as in the case of the larger source Froude number. Again, it reaches a near constant depth at a distance of approximately $5h_o$, after which it evolves much more slowly downstream.

The flux of ambient fluid entrained in this mixing zone could be found by measuring the vertical profile of the horizontal velocity just downstream of the mixing zone and comparing this with the source volume flux. The vertical profile of the horizontal velocity was found by tracking the motion of a series of vertical lines of dye released into the flow. The lateral extent of the mixing zone was found

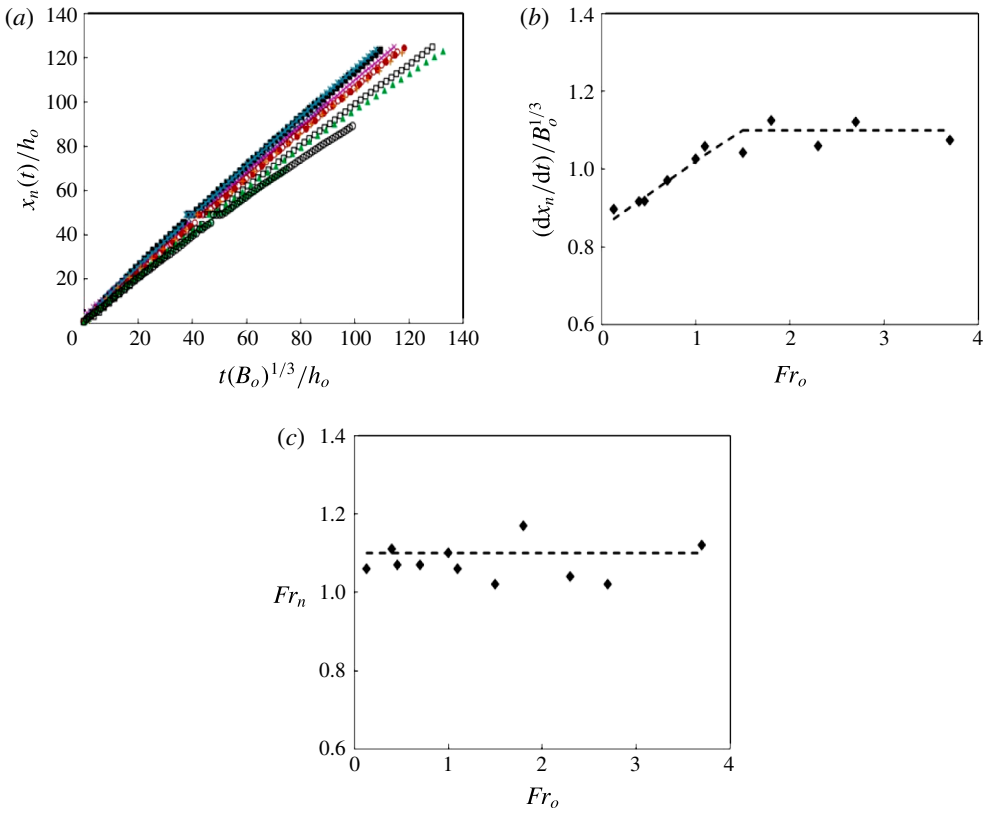

FIGURE 4. Experiments A–K. (*a*) Position of the dimensionless head of the current, $x_n(t)/h_o$, as a function of dimensionless time, $tB_o^{1/3}/h$, for each of the experiments. The symbols for the different experiments are A, black empty circles; B, green solid triangles; C, green empty triangles; D, black empty squares; E, orange pluses; F, red empty circles; G, red solid circles; H, light blue stars; I, pink crosses; J, black solid squares; K, blue empty diamonds. (*b*) Variation of the constant λ as a function of the source Froude number (3.2). (*c*) Variation of the Froude number of the head, Fr_n, as a function of the source Froude number, Fr_o.

by determining the point at which the current depth tended to a more uniform value with position, and the vertical lines of dye were then released downstream of this point. Since the entrainment per unit distance downstream of the inflow mixing zone appeared to be small compared with the mixing in this initial adjustment region (see below), our measurement of the flow was insensitive to the precise location of the point at which we released the dye, provided that this was downstream of but close to the inflow mixing zone. In all cases, the dye was released within a distance of 10–20 cm downstream of the inflow mixing zone, a small distance relative to the 5 m long flume. As the current advanced downstream, our measurements suggest that the volume flux mixed into this near-source region remained approximately constant.

In figure 6, we present the normalised vertical profile of the horizontal velocity, $\hat{u}$, where $\hat{u} = u/u_{max}$, with u_{max} the maximum value of u at this position (dashed line). We also present the normalised concentration, $\hat{c}$, where $\hat{c} = c/c_o$, with c_o the concentration of salt in the source fluid, as a function of normalised height, $\hat{h}$, where $\hat{h} = h/h_{max}$,

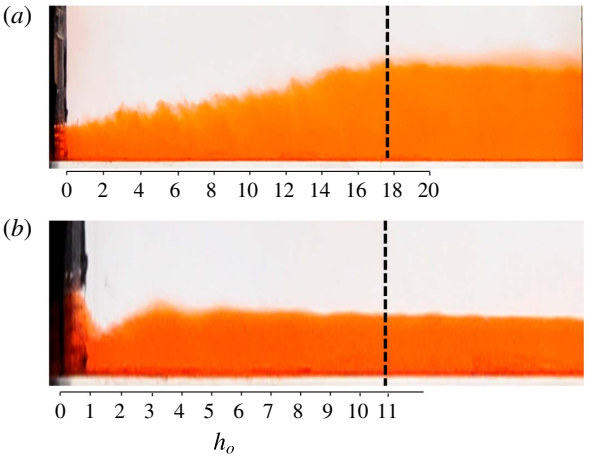

FIGURE 5. Photograph of the current just downstream of the source, in the region $0 < x < 30h_o$, for the cases (*a*) $Fr_o = 2.7$ and (*b*) $Fr_o = 0.4$. In (*a*), the current develops a turbulent mixing zone in the region $0 < x < 20h_o$, reminiscent of an extended hydraulic jump or jet mixing zone, while further downstream the flow depth is more uniform and there is little indication of further turbulent mixing on the upper surface of the current. In (*b*), the flow initially accelerates and plunges on entering the tank, and this is then followed by a turbulent mixing region in which the current slowly deepens over a distance of order $5h_o$. In both cases, downstream of the mixing zone, there is a region of near constant depth. The velocity profiles are measured at the point labelled with the vertical dashed line.

with h_{max} the maximum value of h at this position (solid line). The maximum value of h corresponds to the point at which the concentration falls below the fraction 0.05 of the original source fluid. For reference, we also present the concentration of salt in the head of the current, as measured a distance $0.1x_n$ behind the actual front of the flow, $x_n(t)$ (dotted line). In figure 6, profiles are shown for three source Froude numbers, $Fr_o = 0.4$, 1.5 and 2.7. We integrated the velocity profile to estimate the volume flux, per unit width, in the current downstream of the adjustment zone, Q_m. This was used to estimate the flux of ambient fluid, per unit width, that was mixed into the current in this transition zone, $Q_m - Q_o$, and the ratio $e_{in} = Q_m/Q_o - 1$ is shown in figure 7(*a*) (solid circles). As a check on the accuracy of this measurement, we estimated the buoyancy flux in the current at this point by integrating the product of the velocity and buoyancy over the height of the current. We found that in all experiments this was within 10 % of the source buoyancy flux, per unit width. The data in figure 7(*a*) show that for low Fr_o, there is relatively little mixing in the inflow mixing zone and $e_{in} = 0.2 \pm 0.1$. In this case, the current has a relatively uniform density and velocity with height up to the point at which there is a transition to the overlying ambient fluid (figure 6*a*). As Fr_o increases, there is more entrainment near the source (figure 7*a*), with e_{in} increasing to values of order 0.7 ± 0.1 when $Fr_o = 3.7$. In this case, at points downstream of the inflow mixing zone, the current density and velocity vary continuously over the full depth of the current (figure 6*b*,*c*).

As noted above, in the case that $Fr_o > 1$, then on inflow the flow is supercritical and begins to mix and deepen after entering the tank (figure 5*a*). In contrast, with $Fr_o < 1$, the inflow is subcritical, but on entering the tank, the flow accelerates and thins to become supercritical some distance beyond the inflow (figure 5*b*), and then it

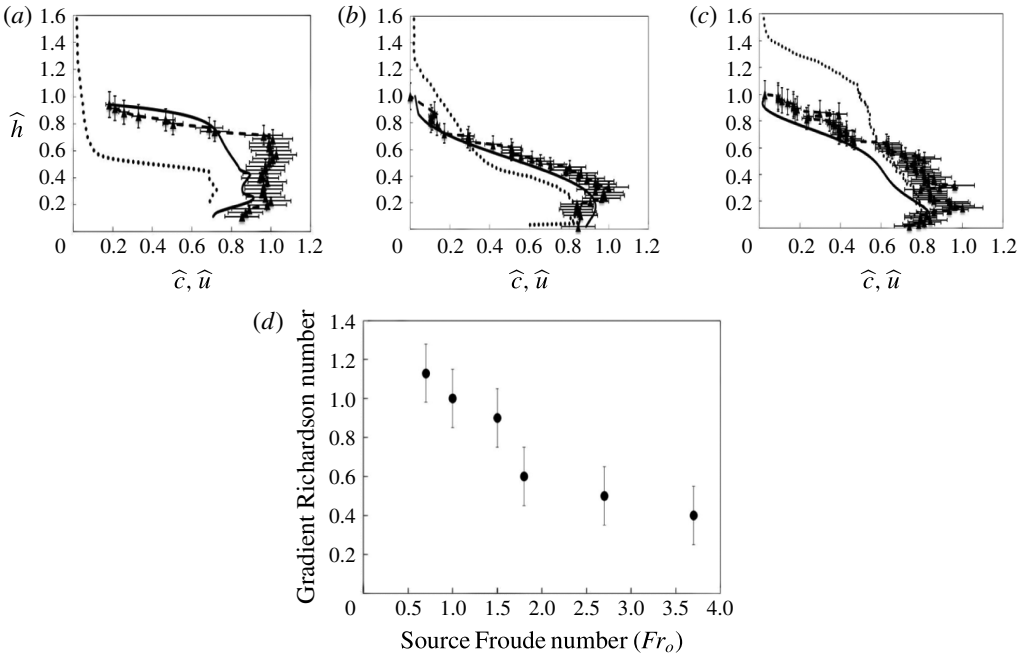

FIGURE 6. (*a–c*) Variation of the vertical profile of salt concentration normalised by the source salt concentration as measured just downstream of the inflow mixing zone (solid line) and at a distance $0.1x_n$ behind the head of the flow (dotted line), and the horizontal speed, normalised by the maximum horizontal speed just downstream of the inflow mixing zone (triangles, dashed line) as a function of normalised height. The height is normalised relative to the total depth of the current at this point. Curves are shown for three source Froude numbers (experiments B3, G3 and J3), illustrating the different profiles of the source current immediately downstream of the mixing region for the cases of small, moderate and substantial mixing in the inflow mixing zone. (*d*) Estimate of the gradient Richardson number in the current just downstream of the inflow mixing zone as a function of the source Froude number.

appears to mix and deepen. Our data reveal that just beyond the inflow mixing zone, the flow has become stratified in velocity and buoyancy, with the lowest part of the flow being of nearly constant speed and density, and the upper part of the flow having a vertical gradient in velocity and buoyancy, below the ambient fluid. The stability of such a region depends on the gradient Richardson number, $Ri_g = \mathrm{d}g'/\mathrm{d}z/(\mathrm{d}u/\mathrm{d}z)^2$, with the flow being stable for $Ri_g > 0.25$ (Turner 1979). If we approximate the density and velocity profiles measured in the current just downstream of the inflow mixing zone (e.g. figure 6) as having an upper region that is linearly stratified in density and velocity and a lower region of constant speed and buoyancy, then we estimate that the gradient Richardson number has a value that increases from 0.4 ± 0.15 when $Fr_o = 3.7$ to 1.15 ± 0.15 as Fr_o decreases to a value of 0.7, as shown in figure 6(*d*). This suggests that downstream of the inflow mixing zone, the current has become stable.

3.3. *Mixing near the head*

We also measured the rate of increase of the total volume of the current, per unit width, as a function of time by calculating the area of the region in which the

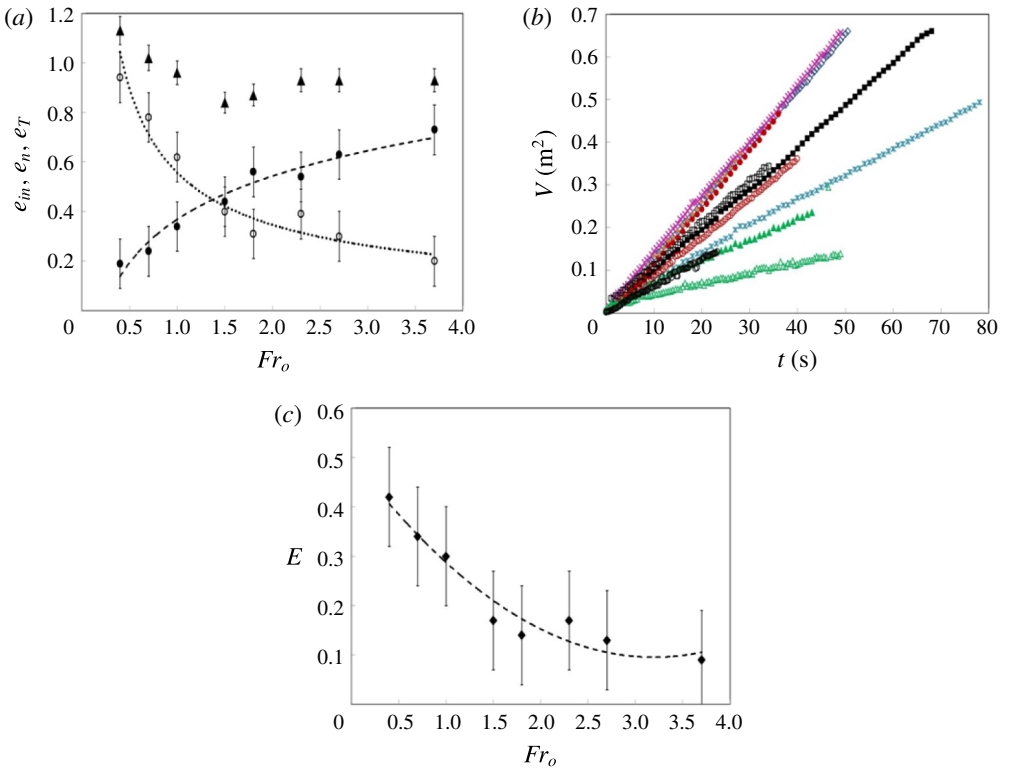

FIGURE 7. (*a*) Variation of the total fractional mixing in the current, $(\mathrm{d}V/\mathrm{d}t)/Q_o - 1$ (solid triangles), the fractional mixing in the inflow region, $e_{in} = Qm/Q_o - 1$ (solid circles), and the fractional mixing in the remainder of the current, e_n ((3.3); open circles), as a function of the source Froude number. (*b*) Total volume of the current per unit width as a function of time. The symbols for the different experiments are A, black empty circles; B, green solid triangles; C, green empty triangles; D, black empty squares; E, orange pluses; F, red empty circles; G, red solid circles; H, light blue stars; I, pink crosses; J, black solid squares; K, blue empty diamonds. (*c*) Variation of the nose entrainment parameter, E, as defined by (3.5), representing the fraction of the fluid initially ahead of the current which is entrained by the current as it is displaced over the head of the current.

concentration of dye is in excess of a threshold value, which we set to be equal to 0.05 of the initial concentration of the source fluid (figure 7*b*). We varied the threshold value used to measure the total volume and we estimate the error in our measurements to be less than 5 % (cf. Sher & Woods 2015). We find that to good approximation, $V(t)$, the volume per unit width, increases linearly with time as the current advances downstream, as shown in figure 7(*b*) for each of the experiments (A–K, table 1). The rate of increase of $V(t)$ with time does not depend strongly on Fr_o, and values in the range $1.8Q_0 < \mathrm{d}V/\mathrm{d}t < 2.1Q_0$ are shown in figure 7(*a*) with solid triangles. This suggests that overall the current fluid is diluted to an average concentration of approximately 0.4–0.55 of the source fluid. If we compare the rate of volume increase in the whole current with the measured volume flux per unit width downstream of the near-source mixing zone, Q_m, we can estimate the rate of entrainment of fluid in the remainder of the flow as a fraction of the source volume

flux,

$$e_n = \frac{\mathrm{d}V/\mathrm{d}t - Q_m}{Q_o}. \tag{3.3}$$

The results of this calculation are shown in figure 7(*a*) (open circles), and illustrate the shifting balance between mixing near the source for large source Froude number and mixing downstream for smaller source Froude number.

If we follow the classical parameterisation for the rate of entrainment of ambient fluid into the upper surface of the flow and take it to be of the form $\alpha(Fr(x,t))u(x,t)$ per unit area, where Fr is a local Froude number for the flow (Ellison & Turner 1959; Dallimore, Imberger & Ishikawa 2001; Chowdhury & Testik 2015), then we would expect the total volume of the current per unit width to increase according to the relation

$$\frac{\mathrm{d}V}{\mathrm{d}t} = Q_o + e_{in}Q_o + \int_{L_o}^{L(t)-L_n} \alpha(Fr(x,t))u\,\mathrm{d}x + e_hQ_o, \tag{3.4}$$

where e_h is the fraction of the mixing that occurs at the head of the flow, in a region of length L_n, say, just behind the head, estimated to be of order 3–5h_n, and L_o is the length of the mixing zone near the inflow, estimated to be of order 5–15h_n. The middle term on the right-hand side then represents the entrainment along the upper boundary of the main part of the current away from the inflow adjustment zone and the head. If this entrainment was significant in our experiments, we would expect a gradual increase in the rate of change of volume with time, since u is nearly constant and $L(t)$ increases linearly with time (cf. Johnson & Hogg 2013). However, our experimental data show that, to good approximation, the volume increases at a rate proportional to t (figure 7*b*). We infer that, for the length scale of the currents explored in this study, which travel 5 m along the flume, corresponding to a distance of order $L(t) \leqslant (50\text{–}100)h_n$, any mixing on the upper surface of the flow is small compared with the sum of the mixing at the source and the nose of the flow, and so $e_h \simeq e_n$.

This interpretation is consistent with our dye experiments (figure 3*b*,*d*), since there is little evidence of vigorous mixing of ambient fluid into the current in the region between the inflow mixing zone and the nose of the flow; indeed, the interfaces that demarcate changes in dye colour appear to remain sharp as they stretch in the direction of flow over time (figure 3). Moreover, the billows and other mixing structures on the upper surface of the flow appear to be much weaker upstream of the near-head mixing zone. In figure 3, we have compared the speed of the relatively dense fluid lower in the current with the speed of the head of the current: in the case of a small source Fr_o, more ambient fluid is mixed into the head, and so the relatively dense fluid in the current takes longer to reach the front of the flow than in the case of larger Fr_o, where less ambient is mixed into the head. This is manifested by a larger difference in speed of the fluid at the base of the current relative to the speed of the head for larger Fr_o, as seen in figure 3.

The quantity e_n (3.3) can be represented in terms of the fraction of the fluid displaced by the head of the gravity current that is mixed into the current, E, according to the balance (Sher & Woods 2015)

$$Eh_n\frac{\mathrm{d}x_n}{\mathrm{d}t} = e_nQ_o. \tag{3.5}$$

The variation of E with Fr_0 is shown in figure 7(*c*). Currents for which $Fr_0 < 1$ involve relatively little mixing near the inflow but have a much larger entrainment

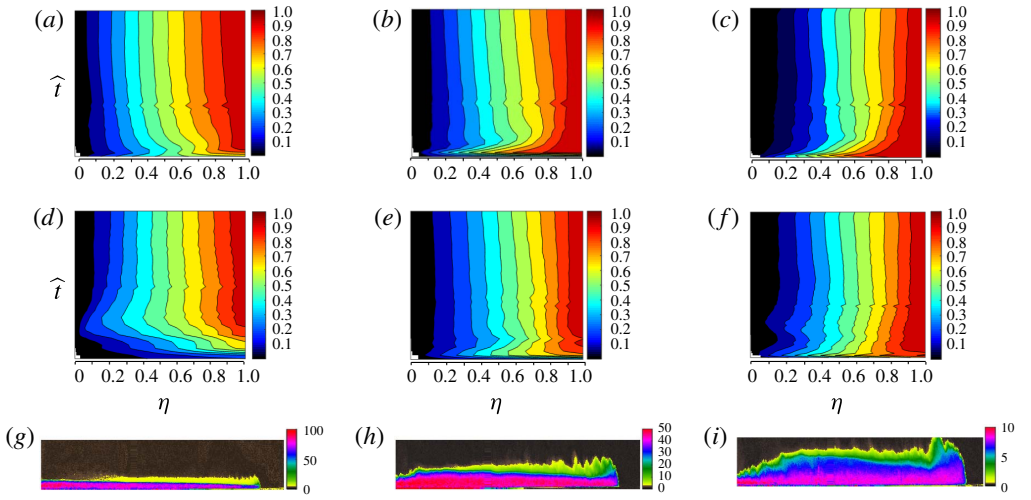

FIGURE 8. The evolution with dimensionless time (y-axis) of contours of (a–c) the fraction of the total volume and (d–f) the fraction of the total buoyancy of the current, in the region $0 < \xi < \eta$, as a function of η (x-axis) for $0 < \eta < 1$. Time is scaled relative to the time to travel a distance equal to the depth of the head of the current. The contours correspond to the values $0.1, 0.2, \ldots, 1.0$. (g–i) Concentration field throughout the current at one instant in time. The image is shown in false colour, with the concentration being given by the scale bar (g kg^{-1}). Measurements are shown for three gravity currents, corresponding to (a,d,g) $Fr_o = 0.4$ (experiment B), (b,e,h) $Fr_o = 1.5$ (experiment G) and (c,f,i) $Fr_o = 2.7$ (experiment J).

at the head of the flow, with E decreasing from 0.4 ± 0.08 to 0.1 ± 0.08 as Fr_0 increases from 0.4 to 3.7. We note that Sher & Woods (2015) found that in the different case of a finite-release gravity current, once the flow becomes self-similar, E has a value in the range 0.6–0.75. For the present experiments, figure 6(d) illustrates that downstream of the initial mixing zone, the gradient Richardson number in the currents becomes progressively larger as Fr_o decreases; this increasing stability of the flow may be related to the greater mixing in the head of the flow, since we also find that E increases as Fr_o decreases. It would be interesting to measure the gradient Richardson number in a finite-release current to establish whether this is also consistent with the greater value of E in such currents.

3.4. *Self-similarity*

Given that our data suggest that the mixing occurs primarily near the inflow and the head of the flow, and that the speed of the flow is nearly constant, we might anticipate that the currents take on a long-time asymptotic self-similar structure in which the distribution of density and volume along the current is primarily a function of the position relative to the nose, $\eta = x/x_n(t)$. Further, we might anticipate that this structure depends on the source Froude number given the different partitioning of the mixing between the inflow and the head and the different vertical structure of the flow. To explore this hypothesis, in figure 8, we show the evolution with dimensionless time (vertical axis) of contours of (a–c) the fraction of the total volume and (d–f) the fraction of the total buoyancy of the current, in the region $0 < \xi < \eta$, as a function of η (horizontal axis) for $0 < \eta < 1$. Time is scaled relative to the time to travel a distance

equal to the depth of the head of the current. The contours of fractional volume and fractional buoyancy correspond to the values 0.1, 0.2, . . . , 1.0. Measurements are shown for three gravity currents, with input Froude numbers of 0.4 (*a*,*d*), 1.5 (*b*,*e*) and 2.7 (*c*,*f*). In each case, there is an initial transition period as the current becomes established after which the contours become nearly independent of time, and the structure of the current then appears to depend primarily on η and Fr_o. It would be interesting to explore how the currents evolve over even greater distances from the source.

For each of the currents in figure 8, in (*g–i*), we illustrate the concentration field throughout the current at one instant in time. In (*g*), with $Fr_0 < 1$, there is less mixing in the inflow adjustment region (figure 7*a*). A relatively dense region of fluid at the base of the flow then advances towards the head of the flow (figure 3*d*). Here, it rises and mixes with the displaced ambient fluid, forming the upper wake region of relatively low density which extends backwards from the nose of the current (figure 8*a*,*d*,*g*). Given the large amount of mixing near the head, the low-density region near the nose occupies a relatively large fraction of the depth of the current; however, as the current continues forward, and new source fluid migrates along the base of the tank, this upper mixed wake region shears out behind the head and hence occupies a progressively smaller fraction of the depth of the flow. In contrast, with higher inlet Froude numbers, there is much more mixing of ambient fluid in the near-source mixing zone (figures 3*a*,*b*; 5*a*). This leads to a much more continuous vertical stratification (figure 6*c*) and there is less mixing of the displaced ambient fluid into the head of the flow (figure 7*a*, figure 8).

4. Discussion

Our experiments have revealed that the structure of a continuous gravity current is strongly controlled by the mixing with ambient fluid near the source and also at the head of the flow. This leads to vertical and horizontal stratification of the density and also a vertical shear in the horizontal velocity. Fluid near the base of the flow travels faster than the head of the current, and continuously supplies the front of the flow with relatively dense fluid. As this rises up over the head, it mixes with some of the ambient fluid originally ahead of the flow front which is also displaced upwards over the head of the current, leading to an upper region in which the density is intermediate between the fluid supplied from the inflow mixing region and the ambient fluid. This upper region travels forward more slowly than the head itself, enhancing the stratification of the current (figures 3, 8). The combination of the mixing at the head and at the inflow leads to dilution of the flow to an average concentration of approximately 0.5 ± 0.05 of the initial concentration, but the partitioning of this mixing between the inflow and the head is strongly dependent on the source Froude number, Fr_o. With small Fr_o, more mixing occurs near the head, while for larger Fr_o, most mixing occurs near the inflow. The Froude number at the head of the flow is of order unity, while the position of the flow front follows a relation of the form $x_n = \lambda B^{1/3} t$ (3.2). It would be of interest to include the mixing and vertical stratification, as observed in our experiments in theoretical models of steady gravity currents, such as presented, for example, by Hogg *et al.* (2016). The vertical stratification is key since it leads to different advection speeds of the buoyancy, mass and momentum, while the mixing at both the inflow and the head is key in generating this stratification and enabling a consistent description of mass conservation.

Our new results concerning the entrainment and dilution in turbulent gravity currents supplied by a steady source of buoyancy illustrate that, even as the flow travels far

from the source, the mean concentration of the fluid near the head of the flow remains high. This has important implications for the hazards associated with gravity currents produced by a continuous source of dense gas or smoke; in contrast, a gravity current produced by a finite release of the same dense gas becomes progressively more dilute with distance from the source (Sher & Woods 2015). We are presently exploring the analogous problem of mixing in particle-laden gravity currents. We also note that the present work focuses on Boussinesq currents in which the density differences are relatively small, as appropriate in many situations (Turner 1979). However, it would be of interest to extend the investigation to explore the effect of larger density differences, as relevant for the dynamics of dense ash flows for example (Bursik & Woods 1996).

Acknowledgements

This work was supported by BP and the BP Institute, University of Cambridge. We are very grateful to the three referees for their helpful comments.

References

BONNECAZE, R. T., HUPPERT, H. E. & LISTER, J. R. 1993 Particle-driven gravity currents. *J. Fluid Mech.* **250**, 339–369.

BRITTER, R. E. 1979 The spread of a negatively buoyant plume in a calm environment. *Atmos. Environ.* **13**, 1241–1247.

BRITTER, R. E. & LINDEN, P. F. 1980 The motion of the front of a gravity current travelling down an incline. *J. Fluid Mech.* **99**, 531–543.

BURSIK, M. & WOODS, A. W. 1996 The dynamics and thermodynamics of large ash flows. *Bull. Volcanol.* **58**, 175–193.

CAFIERO, G. & WOODS, A. W. W. 2016 Experiments on mixing in wakes in shallow water. *J. Fluid Mech.* **804**, 351–369.

CENEDESE, C. & DALZIEL, S. 1998 Concentration and depth fields determined by the light transmitted through a dyed solution. In *Proceedings of the 8th International Symposium on Flow Visualization* (ed. G. M. Carlomango & I. Grant). ISBN 0953399109.

CHEN, J. C. 1980 *Studies on Gravitational Spreading Currents*. Caltech.

CHOWDHURY, M. R. & TESTIK, F. Y. 2014 A review of gravity currents formed by submerged singleport discharges in inland and coastal waters. *Environ. Fluid Mech.* **14**, 265–293.

CHOWDHURY, M. R. & TESTIK, F. Y. 2015 Axisymmetric underflows from impinging buoyant jets of dense cohesive particle-laden fluids. *J. Hydraul. Engng* **141-3**, 1–10.

DALLIMORE, C. J., IMBERGER, J. & ISHIKAWA, T. 2001 Entrainment and turbulence in saline under flow in Lake Ogawara. *J. Hydraul. Engng* **127-11**, 937–948.

ELLISON, T. H. & TURNER, J. S. 1959 Turbulent entrainment in stratified flows. *J. Fluid Mech.* **6**, 423–448.

GRATTON, J. & VIGO, C. 1994 Self-similar gravity currents with variable inflow revisited: plane currents. *J. Fluid Mech.* **258**, 77–104.

GRUNDY, R. & ROTTMAN, J. 1986 Self similar solutions of the shallow water equations representing gravity currents with variable inflow. *J. Fluid Mech.* **169**, 337–351.

HACKER, J., LINDEN, P. F. & DALZIEL, S. B. 1996 Mixing in lock release gravity currents. *Dyn. Atmos. Oceans* **24**, 183–195.

HALLWORTH, M. A., HUPPERT, H. E., PHILLIPS, J. C. & SPARKS, R. S. J. 1993 Entrainment in turbulent gravity currents. *Nature* **362**, 829–831.

HALLWORTH, M. A., HUPPERT, H. E., PHILLIPS, J. C. & SPARKS, R. S. J. 1996 Entrainment in two dimensional and axisymmetric gravity currents. *J. Fluid Mech.* **308**, 289–311.

HOGG, A. J., NASR-AZADANI, M. M., UNGARISH, M. & MEIBURG, E. 2016 Sustained gravity currents in a channel. *J. Fluid Mech.* **798**, 853–888.

HUPPERT, H. E. 2006 Gravity currents: a personal perspective. *J. Fluid Mech.* **554**, 299–322.

HUPPERT, H. E. & SIMPSON, J. E. 1980 The slumping of gravity currents. *J. Fluid Mech.* **99**, 785–799.

JOHNSON, C. & HOGG, A. 2013 Entraining gravity currents. *J. Fluid Mech.* **731**, 477–801.

MARINO, B. M., THOMAS, L. P. & LINDEN, P. F. 2005 The front condition for gravity currents. *J. Fluid Mech.* **536**, 49–78.

MAXWORTHY, T. 1983 Gravity currents with variable inflow. *J. Fluid Mech.* **128**, 247–257.

NAJAFPOUR, N., SAMIE, M., FIROOZABADI, B. & AFSHIN, H. 2014 Theoretical and experimental investigation of density jump on an inclined surface. *Scientia Iranica* B **21-5**, 1655–1665.

NOURMOHAMMADI, Z., AFSHIN, H. & FIROOZABADI, B. 2011 Experimental observation of the flow structure of turbidity currents. *J. Hydraul Res.* **49-2**, 168–177.

OTTOLENGHI, L., ADDUCE, C., INGHILESI, R., ARMENIO, V. & ROMAN, F. 2016 Entrainment and mixing in unsteady gravity currents. *J. Hydraul Res.* **54**, 541–557.

ROTTMAN, J. W. & SIMPSON, J. E. 1983 Gravity currents produced by instantaneous releases of a heavy fluid in a rectangular channel. *J. Fluid Mech.* **135**, 95–110.

SAMASIRI, P. & WOODS, A. W. 2015 Mixing in axisymmetric gravity currents. *J. Fluid Mech.* **782**, R1.

SHER, D. & WOODS, A. W. 2015 Gravity currents: entrainment, stratification and self-similarity. *J. Fluid Mech.* **784**, 130–162.

SIMPSON, J. 1997 *Gravity Currents*. Cambridge University Press.

SLIM, A. C. & HUPPERT, H. E. 2008 Gravity currents from a line source in an ambient flow. *J. Fluid Mech.* **606**, 1–26.

TURNER, J. S. 1979 *Buoyancy Effects in Fluids*. Cambridge University Press.

VARJAVAND, P., GHOMESHI, M., DALIR, A. H., FARSADIZADEH, D. & GORGIJ, A. D. 2015 Experimental observation of saline underflows and turbidity currents, flowing over rough beds. *Can. J. Civ. Engng* **42**, 834–844.